Oxides@C Core−Shell Nanostructures: One-Pot Synthesis, Rational Conversion, and Li Storage Property

Xiaoming Sun,† Junfeng Liu,† and Yadong Li*

Department of Chemistry, Tsinghua University, Beijing 100084, People's Republic of China

Received November 30, 2005. Revised Manuscript Received February 13, 2006

A general and facile one-pot hydrothermal method was developed to prepare oxide@C core−shell nanostructures with carbonaceous polysaccharide shells and oxides (including hydroxides or complex oxides) cores. "Coupled synthesis" or "post-synthesis" approaches can be applied. As-formed particles possess hydrophilic and biocompatible shells and variable cores, thus have promising applications in the areas such as life science or colloid science. The nanostructures can be transformed to a metal@C core/shell structure or hollow carbon structure. Samples were characterized with X-ray diffraction, transmission electron microscopy, high-resolution transmission electron microscopy, electron energy loss spectroscopy, and Fourier transform infrared spectroscopy. Electrochemical characterization on calcined SnO_2@C nanostructures showed unusual reversible Li storage capacities. This implies the structural optimization might provide new opportunities to enhance the properties of solids in nanoscale.

Introduction

Core−shell nanostructures have stimulated great interest in the previous decades because of their tunable surface properties, enhanced optical, electronic, and catalytic properties, and consequent wide potential applications.[1,2] Many advantages are attributed to the core−shell structure. For instance, when nanoparticles are used in biosystems to give optical or magnetic signals (e.g., Au, CdSe, or Fe_3O_4), coating a passive shell comprised of inert materials (e.g., silica or polymer) on the surfaces of colloids can isolate the cores from external chemical environments and prevent their toxicity, biodegradation, or other chemical interactions.[3−6] On the other hand, the cores might support or cooperate with the shells, enhance their properties, or afford composite properties in one system.[7−13]

Very recently, core−shell structured nanoparticles with a carbon shell have stimulated great interest. A series of works have been done on the synthesis of metal@C (e.g., Sn@C, Fe@C) or oxides@C (e.g., V_2O_3@C) nanoparticles.[14−21] These nanoparticles exhibited excellent properties especially in battery application. It was found that carbon coated $CaMoO_4$ would give significantly enhanced reversible Li storage capacities.[14] The cycle performance of nanosized Sn metal particles could be improved by encapsulation in spherical hollow carbon.[15] Carbon hollow structures, typically in the form of capsules converted from their core/shell precursors, exhibited higher current and power density when used as a catalyst support in the direct methanol fuel cell.[16] Many approaches have been explored to synthesize carbon-shelled nanoparticles, such as microemulsion interface polymerization and carbonizatoin,[15,17,18] template synthesis from cellulose chars,[19] sealed reaction at elevated temperature from alkoxides,[20] arc discharge in methane or alcohol,[21] and so forth.

Most of the core−shell structured nanoparticles mentioned above were prepared through the "post-synthesis" encapsulation method.[1−13,15] Otherwise, some special equipment (e.g., arc discharge devices[21] or elevated temperature[16,19,20]) was required for the formation of the core−shell structure. So developing a general and facile method which uses inexpensive, "user-friendly" reagents and safe, easy-operating equipment to synthesize carbon-shelled core−shell nanostructures would open an avenue to exploring the physical

* Corresponding author. Fax: (+86) 10-6278-8765. E-mail: ydli@tsinghua.edu.cn.

† Contributed equally to this work.

(1) Caruso, F. *Adv. Mater.* **2001**, *13*, 11.
(2) Schartl, W. *Adv. Mater.* **2000**, *12*, 1899.
(3) Lu, Y.; Yin, Y. D.; Mayers, B. T.; Xia, Y. N. *Nano Lett.* **2002**, *2*, 183.
(4) Wang, Y.; Teng, X. W.; Wang, J. S.; Yang, H. *Nano Lett.* **2003**, *3*, 789.
(5) Wang, Y. A.; Li, J. J.; Chen, H. Y.; Peng, X. G. *J. Am. Chem. Soc.* **2002**, *124*, 2293.
(6) Gohy, J. F.; Willet, N.; Varshney, S.; Zhang, J. X.; Jerome, R. *Angew. Chem., Int. Ed.* **2001**, *40*, 3214.
(7) Cho, G. J.; Fung, B. M.; Glatzhofer, D. T.; Lee, J. S.; Shul, Y. G. *Langmuir* **2001**, *17*, 456.
(8) Oldfield, G.; Ung, T.; Mulvaney, P. *Adv. Mater.* **2000**, *12*, 1519.
(9) Hirakawa, T.; Kamat, P. V. *J. Am. Chem. Soc.* **2005**, *127*, 3928.
(10) Zhang, Y.; Li, Y. D. *J. Phys. Chem. B* **2004**, *108*, 17805.
(11) Teng, X. W.; Yang, H. *J. Am. Chem. Soc.* **2003**, *125*, 14559.
(12) Teng, X. W.; Black, D.; Watkins, N. J.; Gao, Y. L.; Yang, H. *Nano Lett.* **2003**, *3*, 261.
(13) Yi, D. K.; Selvan, S. T.; Lee, S. S.; Papaefthymiou, G. C.; Kundaliya, D.; Ying, J. Y. *J. Am. Chem. Soc.* **2005**, *127*, 4990.
(14) Sharma, N.; Shaju, K. M.; Rao, G. V. S.; Chowdari, B. V. R.; Dong, Z. L.; White, T. J. *Chem. Mater.* **2004**, *16*, 504.
(15) Lee, K. T.; Jung, Y. S.; Oh, S. M. *J. Am. Chem. Soc.* **2003**, *125*, 5652.
(16) Han, S. J.; Yun, Y. K.; Park, K. W.; Sung, Y. E.; Hyeon, T. *Adv. Mater.* **2003**, *15*, 1922.
(17) Yoon, S. B.; Sohn, K.; Kim, J. Y.; Shin, C. H.; Yu, J. S.; Hyeon, T. *Adv. Mater.* **2002**, *14*, 19.
(18) Jang, J.; Ha, H. *Chem. Mater.* **2003**, *15*, 2109.
(19) Herring, A. M.; McKinnon, J. T.; McCloskey, B. D.; Filley, J.; Gneshin, K. W.; Pavelka, R. A.; Kleebe, H. J.; Aldrich, D. J. *J. Am. Chem. Soc.* **2003**, *125*, 9916.
(20) Pol, S. V.; Pol, V. G.; Gedanken, L. *Chem.—Eur. J.* **2004**, *10*, 4467.
(21) Dong, X. L.; Zhang, Z. D.; Jin, S. R.; Kim, B. K. *J. Appl. Phys.* **1999**, *86*, 6701.

10.1021/cm052648m CCC: $33.50
Published on Web 06/23/2006

and chemical properties of the distinguished nanostructures and extending their applications.

In previous research, we have encapsulated noble metal nanoparticles in carbonaceous microspheres using glucose as the carbon source[22] and got shape and optical property manipulation on inner metal cores.[23,24] Herein, this strategy is extended to develop a general and facile method for preparation of core−shell nanostructures with carbonaceous polysaccharide shells and oxides, including hydroxide or oxide halogenate compound cores.

Experimental Section

All the reagents used were A.R. grade, purchased from Beijing Chemical Reagent Factory.

Coupled Synthesis of $Sb_8O_{11}Cl_2$@C, BiOCl@C, Sb_6O_{13}@C, SnO_2@C, and $MnCO_3$@C Nanoparticles. A total of 10 mmol $SbCl_3$, 10 mmol $BiCl_3$, 1 mmol $SbCl_5$, 0.5−5 mmol $SnCl_2$ (or $SnCl_4$), and 2 mmol $KMnO_4$ were dissolved in 0.5 M aqueous glucose solutions, respectively. After vigorous stirring for 10 min, the suspensions were transferred into autoclaves and kept at 180 °C for 4 h. After reaction, the autoclaves were cooled naturally in air, and the suspensions were isolated by filtration and washed with deionized water and alcohol three times.

Post-Synthesis of FeOOH@C, $Pr(OH)_3$@C, and Fe_3O_4@C Nanoparticles. FeOOH, $Pr(OH)_3$, and Fe_3O_4 nanoparticles were synthesized following previous reports.[25−27] The first two were vigorously stirred and ultrasoniated in aqueous glucose solutions to get even dispersions. However, Fe_3O_4 nanoparticles must be ultrasonicated for 10 min in 0.1 M HNO_3 before being dispersed in the aqueous glucose solution. The suspensions were transferred to autoclaves and kept at 180 °C for 4 h. The rest of the rinse steps were the same as previously described for the coupled synthesis.

Calcination of $Sb_8O_{11}Cl_2$@C and BiOCl@C Nanostructures. The nanoparticles obtained after rinsing were accumulated in an alumina boat, which was set in the hot zone of an alumina tube furnace. The content was heated at 850 °C for 2 h in a high purity argon atmosphere under ambient pressure. Then the furnace was naturally air cooled to room temperature under the protection of argon. Calcination of SnO_2@C was performed following the same steps except the temperatures were altered to designed ones.

Conversion of BiOCl in BiOCl@C to Bi Nanospheres. A total of 0.1 g of BiOCl@C nanoparticles was dispersed in 30 mL of water. Then 5 mL of 80% hydrazine was added. After stirring for 10 min, the suspension was sealed in autoclaves and hydrothermally treated at 180 °C for 10 h. Products were filtered and rinsed with deionized water.

Loading of Ag Nanoparticles on the Surface of $Sb_8O_{11}Cl_2$@C Nanoparticles. Freshly prepared $Sb_8O_{11}Cl_2$@C nanoparticles (50 mg) were ultrasonicated and dispersed in $AgNO_3$ solution (1.0 M, 10 mL). The sonication continued for a total of 10 min, and then the solution was filtrated to erase excess $AgNO_3$. A water rinse was repeated three times before the sample was dispersed in alcohol at the aid of sonication for transmission electron microscopy (TEM) observation.

Characterization. Products were characterized with X-ray diffraction (XRD; Bruker D8 Advance X-ray diffractometer with monochromatized Cu Kα radiation, $\lambda = 1.5418$ Å), TEM (Hitachi H800, operated at 200 kV), high-resolution transmission electron microscopy (HRTEM; JEOL, 2010F, operated at 200 kV), and Fourier transform infrared (FT-IR) spectroscopy (Nicolet 560).

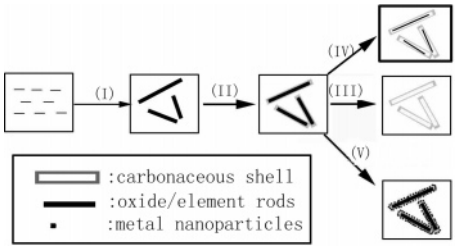

Figure 1. Schematic illustration of one-pot synthesis, conversion, and decoration of oxide@C nanostructures.

Electrochemical Testing. Electrodes were prepared by coating a copper foil substrate with the slurry of the active materials (82 wt %), carbon black (10 wt %), and poly(vinylidene fluoride) (8 wt %) dissolved in cyclopentanone. After coating, the slurry was dried at 100 °C for 12 h and then pressed between two stainless steel plates at 1 MPa. Prior to cell assembling, the electrodes with area of 0.64 cm^2 were dried at 120 °C for 4 h under vacuum. The testing cells had a typical two-electrode construction using a polypropylene microporous sheet as the separator, and 1 M $LiPF_6$ dissolved in ethyl carbonate and diethyl carbonate (1:1, v/v) are used as the electrolyte. A pure lithium foil as the negative electrode and the SnO_2@C nanoparticle film described above are used as the working electrode. The cells were assembled in an argon-filled glovebox. The cells were charged and discharged at a constant current of 0.10 mA and cycled between 0.00 and 2.00 V.

Results and Discussion

The synthesis and conversion strategy of these composite nanostructures are schematically shown in Figure 1. Encapsulation of these inorganic nanoparticles in the carbonaceous shell could be accomplished by "coupled synthesis" or "post-synthesis". Figure 1 shows "coupled synthesis". The starting system is a clear solution of glucose. Other solvable saccharides are also applicable. As hydrolyzable metal salts are introduced into the solution, they hydrolyze and dehydrate at ambient or hydrothermal conditions to form nano- or micro-oxide (or hydroxide, complex oxide) particles (step I, as-formed particles are schematically illustrated as rods). As our previous works have indicated,[22] the saccharides would not carbonize unless the hydrothermal condition overcomes the threshold condition (e.g., time > 2 h at 180 °C), which could accommodate recrystallization or many kinds of chemical reactions. The dissolved saccharides begin to dehydrate and carbonize as the threshold is overcome as evidenced by Raman and IR.[22] As-formed carbonaceous materials encapsulate former oxide particles to form a thin sheath (step II). The mechanism was drawn inspired by the Ag@C core/shell structure formation mechanism we studied.[23] In that case, the Ag core formed first, and the carbonaceous shell formed consequently and covered the Ag core. But for the case of the oxide@C core/shell structure, it was not definitely demonstrated yet. In addition, it is true that formation of the carbonaceous shell could influence the final shape of the particles as demonstrated by experiment. The carbonaceous sheath is penetrable for small molecules such as amine or hydrazine.[23] Thus, the oxide cores can be removed by chemical or thermal means and leaving behind

(22) Sun, X. M.; Li, Y. D. *Angew. Chem., Int. Ed.* **2004**, *43*, 597.
(23) Sun, X. M.; Li, Y. D. *Langmuir* **2005**, *21*, 6019.
(24) Sun, X. M.; Li, Y. D. *Adv. Mater.* **2005**, *17*, 2626.
(25) Chen, M.; Tang, B.; Nikles, D. E. *IEEE Trans. Magn.* **1998**, *34*, 1141.
(26) Wang, X.; Li, Y. D. *Angew. Chem., Int. Ed.* **2002**, *41*, 4790.
(27) Lian, S. Y.; Kang, Z. H.; Wang, E. B.; Jiang, M.; Hu, C. W.; Xu, L. *Solid State Commun.* **2003**, *127*, 605.

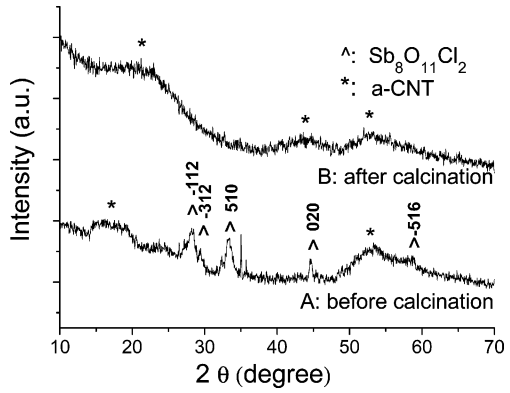

Figure 2. XRD patterns of (A) $Sb_8O_{11}Cl_2$@C nanoparticles and (B) C nanotubes obtained after calcination.

hollow carbonaceous shells as replicas of inner cores (step III). Otherwise, the oxide cores could react with the carbonaceous shell or other introduced chemical reagents to convert to core−shell nanostructures, such as metal@C nanoparticles (step IV). Because carbonaceous shells stem from hydrothermally treated saccharides, rich functional groups could be inherited from starting materials and thus could be used for loading noble metal nanoparticles (step V). Besides hydrolyzation, various chemical reactions can be introduced under aforementioned hydrothermal conditions before carbonization of saccharides. This significantly enriches the accessible core−shell structured nanoparticles.

$Sb_8O_{11}Cl_2$@C Nanoparticles. The $Sb_8O_{11}Cl_2$@C nanoparticle has been studied as the first example. $SbCl_3$ naturally hydrolyzed as it was dispersed in aqueous glucose solutions. The precipitates were further hydrolyzed and crystallized under hydrothermal conditions to form well-crystallized nanorods. These nanorods were encapsulated in the carbonaceous shell as glucose dehydrated under hydrothermal conditions. XRD characterization (Figure 2A) indicated that as-formed nanorods were mainly phase pure $Sb_8O_{11}Cl_2$ (JCPDS 771583). Some unmarked peaks might be due to unknown Sb−O−Cl complex structure. All the $Sb_8O_{11}Cl_2$ nanorods, 60−100 nm in diameter and several micrometers in length, were encapsulated in carbonaceous sheaths (6−10 nm) as revealed by TEM images (Figure 3A,B).

Because complex oxides of Sb, O, and Cl are usually decomposable at a temperature lower than 320 °C and the boiling point of $SbCl_3$ can be as low as 223 °C,[28] the samples tended to transform into hollow structures when they were irradiated by focused electron beams, which was comparable to heating under vacuum. Figure 3A,B showed samples before and after electron beam irradiation for 1 min. The originally fully filled cabonaceous sheath (as marked with an ellipsoid circle in Figure 3A) turned into hollow structures after focused irradiation despite the inner cores being single crystals according to HRTEM and selected-area electron diffraction characterization (Figure 3C,D). Hydroxyl groups distribute all over the shells, because the carbonaceous shells stemmed from glucose in aqueous solution. They could be used to reduce noble metal salt ions.[22] Ag nanoparticles formed after ultrasonication reduction on the surface of the carbonaceous shell (Figure 3E,F) were very small in size (usually <10 nm) because of the mild reaction conditions.

Calcination in noble gas (Ar) to high temperature of 850 °C could drive off the Sb compound cores and carbonize the shells. As formed carbon nanotubes have high purity, uniform shell thickness (∼8 nm) and clear edges (Figure 3G,H). They had essentially the same external size of $Sb_8O_{11}Cl_2$@C nanostructures, indicating a "replica" of $Sb_8O_{11}Cl_2$ nanorod templates. The samples after calcination had localized graphitization zones of ∼2.5 nm in diameter (Figure 3I), exhibiting typical characteristics of "hard carbon", which were obtained from polyol or polyglycol precursors and were hard to graphitize.[29] XRD patterns (Figure 2B) gave very weak peaks corresponding to graphite (JCPDS 751621). Electron energy loss spectroscopy (EELS) recorded on the carbon nanotubes indicated that their profile was similar to that of amorphous carbon (Figure 3J). Two peaks at 284.5 eV and 293.4 eV could be indexed to the π^* and σ^* K-edge peaks of carbon, respectively. The former was stronger than the amorphous one, which might be related to the localized carbonization of samples.

BiOCl@C Nanoparticles. On the basis of the consideration of the chemical reactivity similarity, the synthetic strategy has been extended to prepare BiOCl@C nanoparticles. Figure 4A,B shows the typical TEM images of BiOCl nanorods and nanoplates encapsulated in carbonaceous shells (<10 nm). The nanorods were tens of nanometers in diameter and hundreds of nanometers in length. Plates were also hundreds of nanometers in edge length. After calcination at 850 °C, BiOCl was reduced by a carbonaceous shell to Bi, which led to shrinkage in volume, and left behind many parts of a hollow carbon sheath (Figure 4C,D). When the reduction was carried out in aqueous hydrazine solution at 180 °C, Bi nanospheres would form because of the spacial localization effects of the carbonaceous shell (Figure 4E). This phenomenon indicated that the carbon shell formed after the hydrothermal treatment is still penetrable for small molecules such as hydrazine. It was in accord with our former Ag-dissolving experiment.[23] In comparative experiments, when naked BiOCl nanoparticles were reduced with hydrazine in autoclaves, micrometer sized irregular particles could form. XRD characterization indicated that both the samples were phase pure (Figure 4F). Following the synthetic strategy, TiO_2@C nanoparticles can be prepared using $TiCl_4$ as the starting material (see Supporting Information). In addition, if $SbCl_3$ and $SnCl_4$ were added simultaneously, composite oxides could be prepared in the carbonaceous shell (see Supporting Information).

Adjustment of Sb and Sn Valence States. Because glucose is a mild reducing reagent, it may show the oxidizability when strong reducing agents are introduced. Otherwise, its reducibility will be shown if relatively strong oxidizing agents are introduced. Thus, the valence state of final oxides can be "self-adjusted" by glucose. When $SbCl_5$ was hydrolyzed and hydrothermally treated in glucose

(28) An, J. J.; Chen, Z. C. *Inorganic Compound Synthesis Handbook*; Chemical Engineering Publisher: Beijing, China, 1986, 1st Edition, ISBN I5063-3726.

(29) Wang, Q.; Li, H.; Chen, L. Q.; Huang, X. J. *Solid State Ionics* **2002**, *152*, 43.

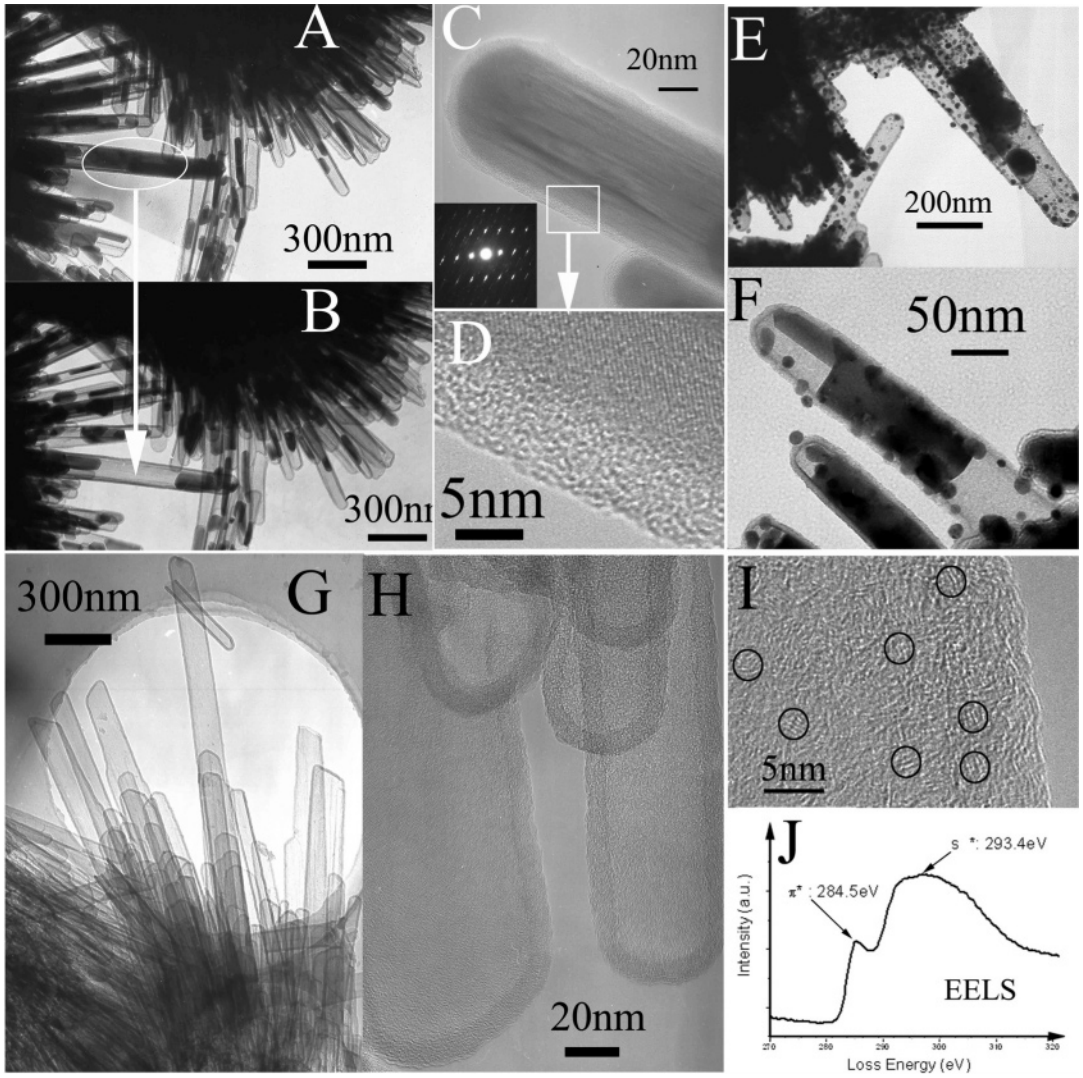

Figure 3. TEM and HRTEM images of $Sb_8O_{11}Cl_2$@C nanoparticles: (A) A typical initial sample; (B) the same sample with the inner core volatilized under electron beam irradiation; (C and D) HRTEM images, (inset) corresponding electron diffractions; (E) Ag nanoparticles-doped sample; (F) sample before doping; (G) pure amorphous carbon nanotubes obtained by thermally driving out the inner cores; (H) HRTEM image of a bundle of nanotubes; (I) partly magnified image to show the local crystallinity; and (J) EELS spectrum of C nanotubes.

solutions, they would convert to Sb_6O_{13} (upper curve in Figure 5, JCPDS 330111). When $SnCl_2$ was introduced into the aqueous solution, SnO_2 would form (bottom curve in Figure 5, JCPDS 770448).

TEM and HRTEM characterizations gave structural information for SnO_2@C nanoparticles prepared from $SnCl_2$ (Figure 6). General images of the nanostructures indicated submicrometer branch-like frameworks (Figure 6A,C). Partly magnified images (Figure 6B,D) revealed actual core−shell structures for each "branch". The samples were tilted by ±25° to ensure that the nanoparticles were encapsulated in the carbon shell rather than attached on the surface. The shape of SnO_2 nanoparticles encapsulated can be tuned by adjusting the $SnCl_2$ concentration. For instance, ∼4 nm roughly round particles formed when 0.1 g of $SnCl_2$ was added (Figure 6B), whereas nanorods ∼10 nm in length formed when 1.0 g $SnCl_2$ was added (Figure 6D). The nanoparticles and nanorods aggregated and were encapsulated by the surrounding carbonaceous bulk solids.

Both the samples exhibited essentially the same XRD patterns (Figure 7A). When calcined at relatively low temperature (400 and 500 °C), the grain size of SnO_2 nanoparticles increased but no new phase formed (Figure 7B,C). TEM images indicated that samples after calcination remained core−shell structures approximately the same as the precursive products despite the SnO_2 proportion getting smaller (Figure 6E) or bigger (Figure 6F). HRTEM images gave further insight into the SnO_2@C nanostructure after calcination: the central parts of the nanostructure comprised a large number of ellipsoidal nanoparticles (Figure 6G); at the edge, very short nanorods could be observed (Figure 6H). These images indicated some anisotropic growth tendency of SnO_2 nanoparticles, which might be attributed to the anisotropic growth and dynamic diffusion process during formation of SnO_2 nanocrystals.

The carbon thermal reduction of SnO_2 could take place when the calcination temperature reached 600 °C. The Sn element emerged as a new phase in XRD patterns (Figure 7D). At the same time, SnO_2 peaks in the XRD pattern were significantly sharpened. This implied that the existence of elemental Sn might accelerate the SnO_2 grain size growth. After calcination at 700 °C for 2 h, the conversion from SnO_2

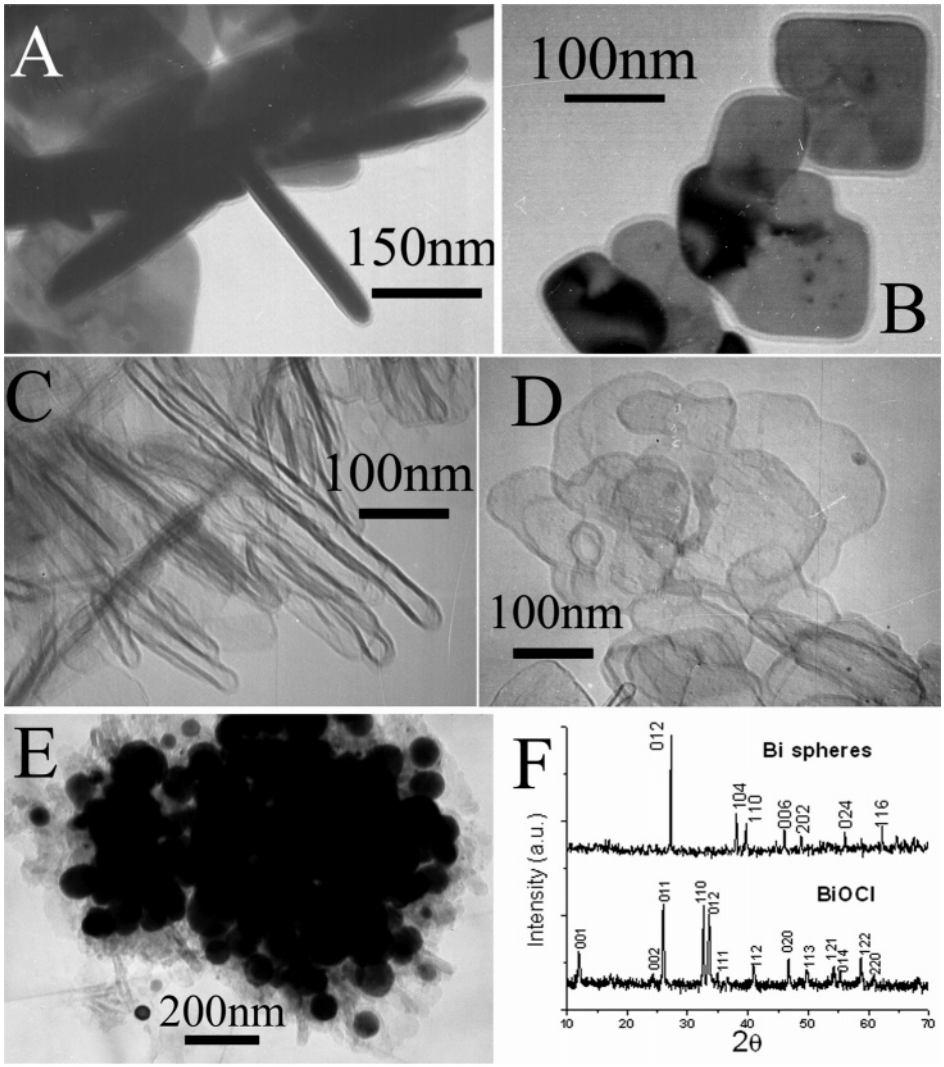

Figure 4. (A and B) Typical TEM images of BiOCl nanorods and nanoplates encapsulated in amorphous carbonaceous shells; (C and D) typical TEM images of the hollow carbon sheath formed after calcination at 850 °C; (E) Bi nanospheres formed when BiOCl@C was reduced by hydrazine; and (F) XRD patterns of the samples.

to Sn was almost complete (Figure 7E). TEM characterization indicated formation of Sn@C nanostructures (Figure 6I).

$MnCO_3$@C Nanoparticles. The redox reaction induced precipitation and encapsulation could be applied not only on the main-group metal but also on the transition metal compounds. The synthesis of $MnCO_3$@C nanoparticles gave a good example. As soon as $KMnO_4$ and glucose were mixed at room temperature, the following reaction took place:

$$24MnO_4^- + 5C_6H_{12}O_6 + 6H_2O \rightarrow 24Mn(OH)_2 + 24OH^- + 30CO_2$$

As-formed $Mn(OH)_2$ could convert to phase pure $MnCO_3$ under hydrothermal conditions (Figure 8A). Carbonization of residual glucose could lead to encapsulation of the $MnCO_3$ particles to form $MnCO_3$@C nanoparticles (as shown in Figure 8B). Recrystallization of inner cores under hydrothermal conditions could densify the cores and produce a separating air layer between the $MnCO_3$ cores and the carbonaceous shell (Figure 8C). After ultrasonication in 0.1 M HCl for 10 min and aging overnight, the core−shell structures turned hollow because of the removal of inner cores (Figure 8D,E).

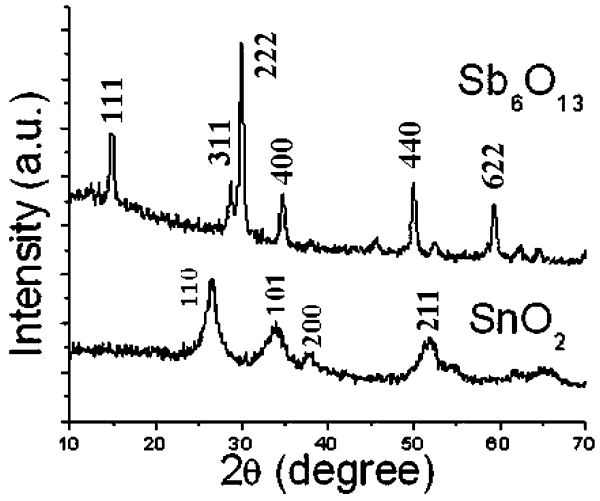

Figure 5. XRD patterns of Sb_6O_{13} (upper) and SnO_2 (bottom) obtained after hydrothermal treatment in an aqueous glucose solution.

From Coupled Synthesis to Post-Synthesis Encapsulation. To further enrich the accessible types of compounds@C core−shell structures, the synthesis strategy was extended from "coupled synthesis" to "post-synthesis" encapsulation.

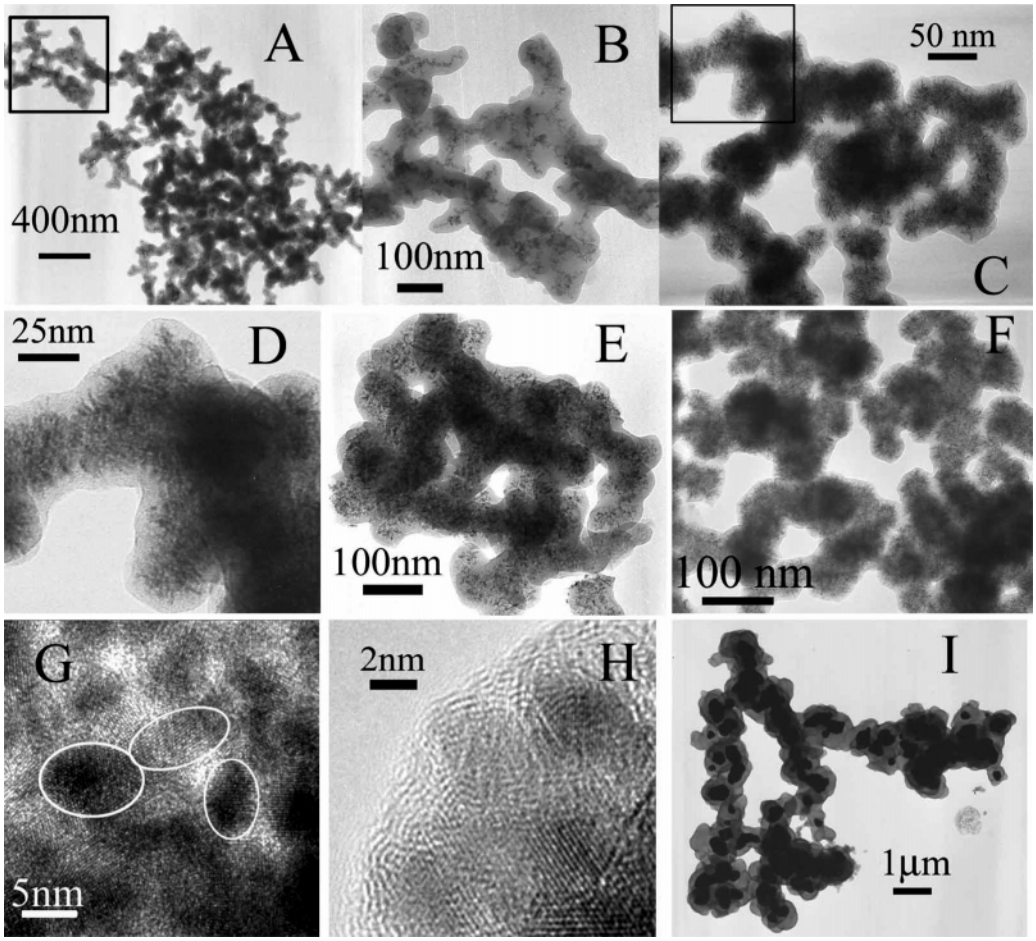

Figure 6. (A and B) TEM images of SnO_2@C nanoparticles with 0.1 g of $SnCl_2$ used for hydrolyzation; (C and D) TEM images of SnO_2@C nanoparticles with 1.0 g of $SnCl_2$ used for hydrolyzation; (E) typical TEM image of the same sample as in part B after calcination at 500 °C for 2 h; (F) typical TEM image of the same sample as in part D after calcination at 500 °C for 2 h; (G and H) HRTEM images of the same sample as in part F; and (I) typical TEM image of the same sample as in part D after calcination at 700 °C for 2 h.

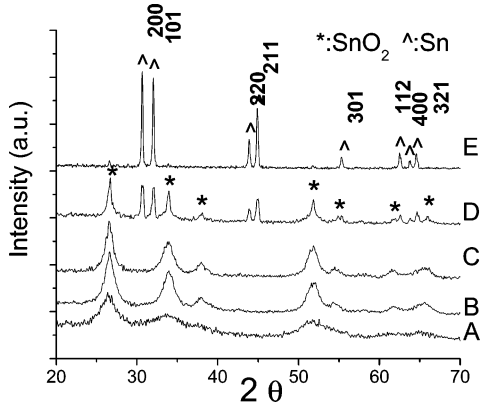

Figure 7. XRD patterns of SnO_2@C nanoparticles: (A) hydrothermally treated sample; (B) sample calcined at 400 °C for 2 h; (C) sample calcined at 500 °C for 2 h; (D) sample calcined at 600 °C for 2 h; and (E) sample calcinated at 700 °C for 2 h.

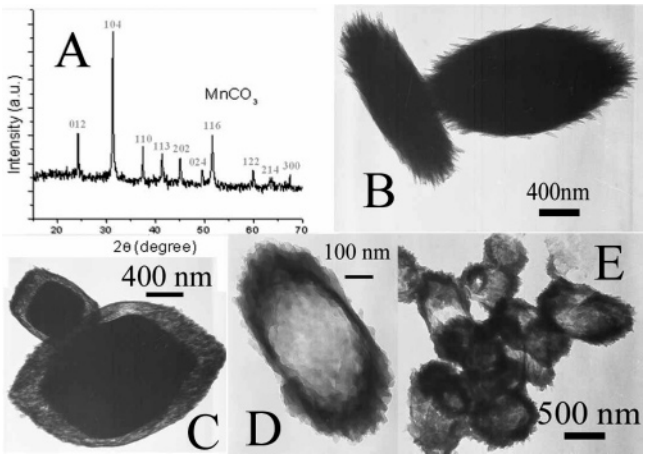

Figure 8. (A) XRD pattern; (B and C) TEM images of $MnCO_3$@C core−shell structured particles; and (D and E) TEM images of the carbonaceous shell left behind after core removal.

Some examples of oxide@C or hydroxide@C are shown below.

Encapsulation of $Pr(OH)_3$ nanorods was investigated as the first example. Figure 9A showed the TEM image of the nanorods synthesized in concentrated KOH solution.[26] After encapsulation in glucose solution under the hydrothermal condition, sheathes (∼8 nm) formed on the hydroxide nanorods cores (Figure 9B). The partially magnified image indicated that the sheath was smooth, uniform, and covering the core entirely (inset in Figure 9B). Acid washing could remove the cores and leave behind carbonaceous sheathes, that is, the nanotubes (Figure 9C). Rice-like FeOOH ellipsoidal nanoparticles could be encapsulated in the carbonaceous shell through a similar procedure (Figure 9D).

In contrast to the encapsulation of hydroxides or hydroxyl oxides that possess rich hydroxyl groups on the surface, encapsulation of oxides required a process of activation. If

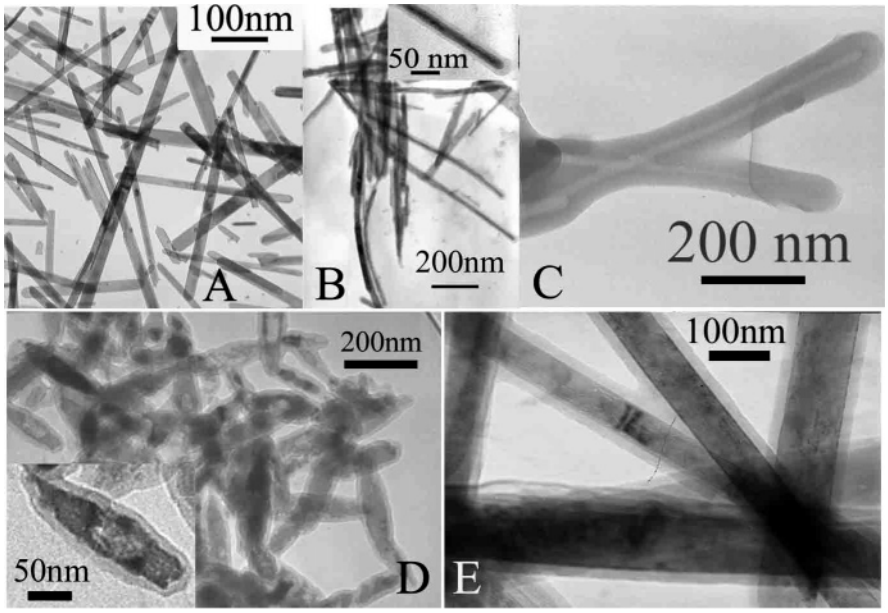

Figure 9. TEM images of (A) raw $Pr(OH)_3$ nanorods; (B) $Pr(OH)_3$@C nanorods; (C) carbonaceous nanotubes left behind after removal of inner $Pr(OH)_3$ nanorods; (D) FeOOH@C nanoparticles; and (E) Fe_3O_4@C nanorods.

not, carbonaceous microspheres rather than core−shell structured nanoparticles could form accompanying naked oxide nanoparticles. According to our preliminary experimental results, the carbonaceous shell seemed to have weak acidity and tended to adhere on basic surfaces with rich hydroxyl groups (e.g., FeOOH). The surface redox reaction could induce the in situ precipitation of carbonaceous units to form sheaths profitably. The Fe_3O_4@C nanoparticle is another example. The Fe_3O_4 nanorods prepared following the coprecipitation method in basic solutions were immersed in 0.1 M HNO_3, H_2SO_4, and HCl solutions, respectively, to activate the particle surface. Only those particles activated in HNO_3 were coated with uniform carbonaceous sheaths (Figure 9E). This implied that the redox reaction between adsorbed nitrate ions and glucose on the oxide surface might facilitate the carbonaceous coating process. Generally speaking, the chemical interactions of the surface functional groups and the coating agents were critical for encapsulation.

Li Storage Property of SnO_2@C Nanoparticles. Encapsulation of compound nanoparticles in a nontoxic carbonaceous shell could effectively endow rich functional groups on the surface and consequent promising applications of the core/shell particles in the areas such as biology or diagnostics. In addition to that, the encapsulation of oxide particles in carbonaceous sheaths also provides an opportunity to investigate the distinct properties of the composite nanostructures. An example for SnO_2@C core−shell nanostructure is shown below.

It is well-known that Sn, SnO_2, and hard carbon from saccharides are all Li storage materials.[15,29,30] Metallic Sn has a theoretical specific capacity of 992 mA·h/g, which is much higher than that of already-commercialized graphite (∼350 mA·h/g).[15] However, its (and its alloy's) commercial use are hindered by their drastic volume variation during Li insertion/extraction cycles, which leads to fast capacity fading.[15,31] Amorphous composite tin oxide materials seem able to overcome the disadvantages[30] where Li was stored by a two-step reaction mechanism:[32−34] lithium first reacts with tin oxide to produce amorphous Li_2O and Sn irreversibly (formula 1) and then Sn alloys with Li reversibly (formula 2). The Li_2O matrix acts as a buffer and dispersive medium for nanosized Sn grains, which is critical for improving the circling performance. Inactive glass-forming elements such as B or P act as a stabilizer to improve the cyclic performance further.[30,35,36]

$$2Li^+ + SnO\ (\text{or } SnO_2) + 2e^- \rightarrow Sn + Li_2O \qquad (1)$$

$$xLi^+ + Sn + xe^- \rightarrow Li_xSn \qquad (x \le 4.4) \qquad (2)$$

$$yLi^+ + C_6 + ye^- \leftrightarrow Li_yC_6 \qquad (y \le 4.4) \qquad (3)$$

It is obvious that if the buffer medium itself has Li storage capacities and high electronic conductivity, the capacity of the composite tin oxide anodes could be further enhanced. The carbonaceous matrix from glucose was demonstrated to be an excellent candidate.[29,37]

Figure 10A showed the charge and discharge curves of SnO_2@C core−shell nanostructures after calcination at 400 °C for 200 min. The anode in the first discharge process had a long potential plateau and a large capacity loss (∼55%). It could be attributed to the irreversible reaction 1 and

(30) Idota, Y.; Kubota, T.; Matsufuji, A.; Maekawa, Y.; Miyasaka, T. *Science* **1997**, *276*, 1395.
(31) Yang, J.; Winter, M.; Besenhard, J. O. *Solid State Ionics* **1996**, *90*, 281.
(32) Courtney, I. A.; Dahn, J. R. *J. Electrochem. Soc.* **1997**, *144*, 2045.
(33) Liu, W. F.; Huang, X. J.; Wang, Z. X.; Li, H.; Chen, L. Q. *J. Electrochem. Soc.* **1998**, *145*, 59.
(34) Li, H.; Huang, X. J.; Chen, L. Q. *Electrochem. Solid State Lett.* **1998**, *1*, 241.
(35) Hayashi, A.; Nakai, M.; Tatsumisago, M.; Minami, T.; Katadab, M. *J. Electrochem. Soc.* **2003**, *150*, A582.
(36) Wan, K. B.; Li, S. F. Y.; Gao, Z. Q.; Siow, K. S. *J. Power Sources* **1998**, *75*, 9.
(37) Xing, W. B.; Dunlap, R. A.; Dahn, J. R. *J. Electrochem. Soc.* **1998**, *145*, 62.

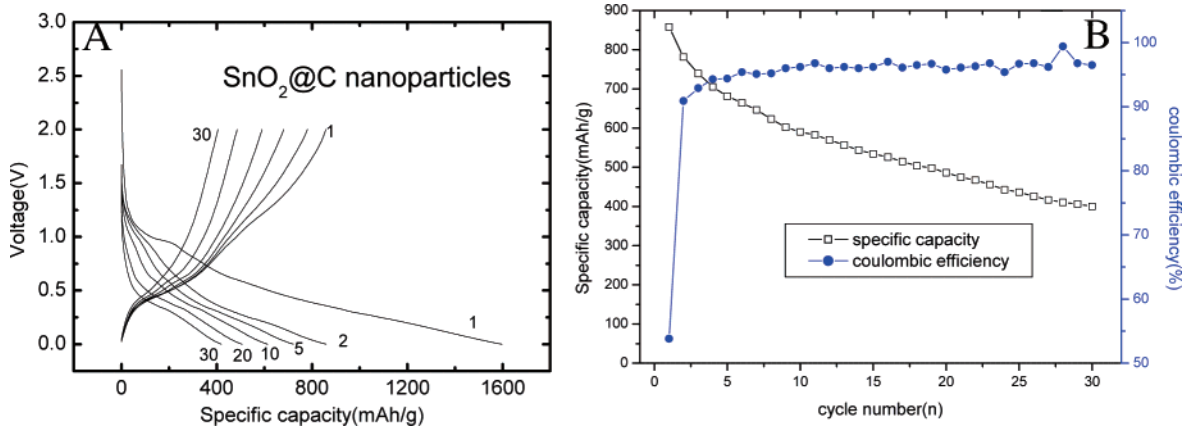

Figure 10. (A) Electrochemical performance of the SnO_2@C nanoparticles electrode in a test Li battery. (B) Relationship between the specific discharge capacity (black) and Coulombic efficiency (blue) and the cycling number.

irreversible trapping of lithium by the carbonaceous matrix. The latter might relate to the surface ([H], [O], etc.) reaction and solid electrolyte interface formation.[38]

However, the reversible capacity of the second discharge process (857 mA·h/g) was far beyond our expectation. SnO_2 has a theoretical specific reversible capacity of 786 mA·h/g. According to the thermogravimetric analysis (TGA) results, SnO_2 was ∼46% in weight content. That means the specific capacity from SnO_2 should not exceed 361 mA·h/g. The rest of the carbon should contribute 496 mA·h, corresponding to 918 mA·h/g carbon. It is known that the reversible Li storage capacity of hard carbon is hard to beyond 600 mA·h/g.[39] According to experimental results, the second discharge capacity of nano-SnO_2 prepared following the same hydrothermal (180 °C) and thermal (400 °C, 200 min) procedure was only 681 mA·h/g, and that of hard carbon following the same procedure was only 156.6 mA·h/g. Both of the samples faded quickly (see Supporting Information, Figure s8). Where do the excessive capacities come from?

Some precursive work on SnO_2 anodes provided some hints to give elucidation. It has been reported that transition metal oxides show reversible Li storage behaviors.[40] In those cases, a transition metal can react with Li_2O upon Li extraction. That means reaction 1 is reversible, which contributes very high reversible capacity. Up to now, no experimental evidence shows whether reaction 1 for Sn-based oxides is completely irreversible or not. However, one paper has mentioned that Li−O bonds are not stable when the charging voltage is above 1.3 V.[41] A recent work indicated that reaction 1 for most of metal compounds is reversible in view of the thermodynamics, and the theoretic voltage for SnO_2 is 1.5 V. The reversal of reaction 1 from LiX (e.g., Li_2O) and metal (e.g., Sn) back to metal compounds is mainly influenced by the intrinsic conductivity of MX compound, grain size of LiX and metal, separated distance between LiX and metal, and electronic contact with conductive additive.[42]

SnO_2 is a good semiconductor. The decomposed product from tin oxides is a nanocomposite as evidenced before.[34,43,44] For the SnO_2@C core−shell nanostructures, the SnO_2 nanoparticles are embedded in the carbonaceous shell, which ensures that formed Li_2O and Sn contact well without other separation. In addition, internal Li_2O/Sn products are electronically contacted directly with the carbonaceous shell during cycling. This provides a kinetic advantage for the reverse reaction 1. We believe that reaction 1 is at least partially reversible in our case, which contributes to the unusually high reversible capacity.

The cyclic performance of the as-prepared SnO_2@C material is not satisfying, which may need further optimization. Despite that, this result illustrates a good prospect that the capacity of oxide anodes may be significantly enhanced by optimized microstructure. Moreover, because many transition-metal compounds have been demonstrated as promising high-capacity negative-electrode materials for lithium-ion batteries,[40,42] there still exists plenty of room for oxide@C core−shell composite structures in Li storage properties. Further research is in process.

Conclusion

Several types of oxide@C nanostructrues were synthesized in one pot, following "coupled synthesis" or "post-synthesis" approaches. The methods can be extended to the synthesis of core−shell structures of other types of compounds such as composite oxides, sulfides, nitrides, carbides, or metal. It also provided an opportunity to synthesize carbide or carbide-shelled nanostructures. Because the particles possess hydrophilic and biocompatible shells and variable cores, their applications in the areas such as life science or colloid science are promising. SnO_2@C nanostructures showed unusual reversible Li storage capacities. This implies that the structural optimization might provide new opportunities to enhance the properties of solids in nanoscale.

Acknowledgment. The authors truly thank Dr. Hong Li and Prof. Joseph F. Chiang for helpful discussions and Mr. Jie Shu

(38) Winter, M.; Besenhard, J. O.; Spahr, M. E.; Novak, P. *Adv. Mater.* **1998**, *10*, 725.
(39) Dahn, J. R.; Zheng, T.; Liu, Y. H.; Xue, J. S. *Science* **1995**, *270*, 590.
(40) Poizot, P.; Laruelle, S.; Grugeon, S.; Dupont, L.; Tarascon, J. M. *Nature* **2000**, *407*, 496.
(41) Courtney, I. A.; Dahn, J. R. *J. Electrochem. Soc.* **1997**, *144*, 2943.
(42) Li, H.; Balaya, P.; Maier, J. *J. Electrochem. Soc.* **2004**, *151*, A1878.
(43) Brousse, T.; Retoux, R.; Herterich, U.; Schleich, D. M. *J. Electrochem. Soc.* **1998**, *145*, 1.
(44) Retoux, R.; Brousse, T.; Schleich, D. M. *J. Electrochem. Soc.* **1999**, *146*, 2472.

for electrochemical measurements. This work was supported by NSFC (90406003, 20401010, 50372030, 20025102, 20131030), the Foundation for the Author of National Excellent Doctoral Dissertation of P.R. China, and the state key project of fundamental research for nanomaterials and nanostructures (2003CB716901).

Supporting Information Available: Three TEM images, three XRD patterns, three specific capacity vs circling time curves, a FT-IR spectrum, and TGA curves. This material is available free of charge via the Internet at http://pubs.acs.org.

CM052648M